Submitted: Neural Computation

See Globally, Spike Locally: Retinal Oscillations Encode Large Features

Gregory J. Stephens[1,3], Sergio Neuenschwander[4], John S. George[1,3], James Theiler[2,3], David W. Marshak[5], Wolf Singer[4], Garrett T. Kenyon[1,3]

[1]Biological and Quantum Physics (P-21), [2]Space and Remote Sensing Sciences (NIS-2), [3]Los Alamos National Laboratory, Los Alamos, NM, 87545; [4]Max-Planck-Institut für Hirnforschung, Deutschordenstraße 46, 60528-Frankfurt am Main, Germany; [5]Department of Neurobiology and Anatomy, University of Texas Medical School, Houston, TX, 77030,

Abbreviated Title: Encoding Role for Retinal Oscillations

Corresponding Author:
Garrett T. Kenyon
P-21 Biological and Quantum Physics, MS D454
Los Alamos National Laboratory
Los Alamos, NM 87544
phone: 505-667-1900
fax: 505-665-4507
email: gkenyon@lanl.gov

Acknowledgements: The authors wish to acknowledge useful discussions with Chris Wood and Bryan Travis. This work was supported by the Department of Energy Office of Nonproliferation Research and Engineering, the MIND Institute for Functional Brain Imaging, National Eye Institute #EY06472, the National Institute of Neurological Disease and Stroke #NS38310, and by the Lab Directed Research and Development Program at the Los Alamos National Laboratory.

Abstract

High-frequency oscillations evoked by large stimuli have been observed in a variety of vertebrate retinas, but their role in visual function remains unresolved. Here, we hypothesize that coherent oscillations in the spike trains of neighboring retinal ganglion cells encode global topological properties, such as size, that cannot be deduced locally from their mean firing rate. We analyzed the single-trial responses of cat ganglion cells to spots of various sizes and found that the mean spectral amplitude between 75-95 Hz, computed from multi-unit spike trains 50-300 msec in duration, provided good discrimination (70% to 90%) between large and small spots. While the strong size dependence of retinal oscillations has been previously observed, our study demonstrates that size information is encoded on single-trials and short time scales, a necessary condition for such information to be behaviorally relevant. To examine whether the information content of retinal oscillations depends strongly on the underlying mechanism giving rise to them, we constructed two mathematical models: 1) a simple empirical rate-modulated Poisson process and 2) a semi-realistic integrate-and-fire feedback circuit based on retinal anatomy. For each model, the *trial-averaged* oscillatory behavior was matched to that observed experimentally. In addition, the model firing rates were held constant with stimulus size and thus conveyed no topological information. In both models we found single-trial encoding similar to that seen experimentally. We suggest that coherent high frequency oscillations between retinal ganglion cells provide a mechanism for labeling local regions that are part of large visual features.

Introduction

High frequency oscillations have been observed in several vertebrate retinas, including cat (Steinberg, 1966; Laufer & Verzeano, 1967; Neuenschwander & Singer, 1996; Neuenschwander et al., 1999), rabbit (Ariel et al., 1983), mudpuppy (Wachtmeister & Dowling, 1978), frog (Ishikane et al., 1999), macaque (Frishman et al., 2000) and human (Wachtmeister, 1998; De Carli et al., 2001). Nevertheless, the role of oscillatory retinal activity in normal visual processing remains unresolved. Here, we used both experimental and model spike trains to examine how coherent oscillations among neighboring retinal ganglion cells might encode global stimulus properties not locally available in their firing rates. While ganglion cell firing rates typically depend on stimulus size, increasing for spot sizes smaller than the receptive field center and decreasing thereafter due to surround inhibition, modulations in the local mean spike activity cannot be disentangled from changes due to increasing or decreasing contrast. High frequency oscillations, on the other hand, are not evoked by small spots (Ariel et al., 1983; Ishikane et al., 1999; Neuenschwander et al., 1999) and thus are not intrinsically confounded by local contrast. Unlike information encoded by temporal synchrony, which is susceptible to contamination from chance coincidence and therefore potentially unreliable when the firing rate is high (Shadlen & Movshon, 1999), oscillations become easier to detect as the mean firing rate increases.

Here we hypothesize that the average firing rate in a small group of neighboring ganglion cells conveys information only about local stimulus properties, such as luminance contrast, while their coherent high frequency oscillations convey additional information about the global properties of the stimulus such as size. To test this

hypothesis, we asked whether global topological information could be extracted from the coherent oscillations among neighboring retinal ganglion cells upon single stimulus presentations. The answer to this question both constrains and informs the functional role of retinal oscillations. In particular, any information contained in oscillations must be accessible on time scales of the order of 100 msec in order to be behaviorally relevant. Furthermore, the relatively low convergence of retinal neurons at early processing stages precludes averaging over large numbers of cells. If size-dependent oscillations cannot be extracted from a relatively small number of ganglion cells on single stimulus trials, then it is unlikely that such oscillations could be functionally relevant at early processing stages. On the other hand, by demonstrating that retinal oscillations convey global topological information that could be extracted early in the visual processing hierarchy, we can establish the plausibility of this processing mechanism.

We present a re-analysis of multi-unit spike trains from the cat retina that supports this hypothesis. A discrimination analysis was performed between small and large spots on the basis of short sections of multi-unit spike train data, from 50 to 300 msec in duration and containing on the order of 4 to 5 ganglion cells located at the center of the stimulus. Frequency spectra were computed from the individual epochs of multi-unit data and the average amplitude between 75 and 95 Hz was measured relative to baseline after normalizing by the total number of spikes. Despite the presence of substantial single-trial variability, it was possible to discriminate between large and small stimuli, with performance levels between 70 and 90% depending on the length of the analysis window.

We used theoretical models to obtain additional insight into the experimental data. An important question is whether the single trial discrimination mediated by experimentally recorded spike trains results from highly specialized processing, or is instead a general property of coherent oscillations that would likely be present regardless of the underlying mechanism. We therefore analyzed an equivalent single-trial discrimination task using two very different models for generating spatial-temporal correlations. In both models, the firing rate was held constant across stimulus conditions. Because different sized spots evoked different mean firing rates in the experimentally recorded spike trains, it was important to ensure that changes in the mean firing rate did not contribute to the discrimination task. In both models, the size-dependent temporal correlations were similar to those measured experimentally. In the first model, temporal correlations between the separate elements contributing to the multi-unit spike train arose from a common oscillatory modulation of their instantaneous firing probabilities, but the elements themselves did not interact. In the second model (Kenyon et al., 2003), coherent oscillations arose from feedback interactions between ganglion cells and amacrine cells based on circuitry consistent with retinal anatomy (Dacey & Brace, 1992; Vaney, 1994; Jacoby et al., 1996). Similar performance on the size discrimination task was obtained regardless of which mechanism was used to generate model spike trains. The models also allowed us to detail how the discrimination task depended on the length and number of neighboring cells included in the multi-unit record, an analysis that could not be performed with the existing experimental data.

Methods

Physiological Recordings:

Data from previously reported experiments in the cat retina were reanalyzed in order to quantify the information relating to the global stimulus topology conveyed by high frequency oscillations in short sections of multi-unit spike train data. As no new experiments were conducted, and since a detailed description of the experimental methods is available elsewhere (Neuenschwander et al., 1999), only an abbreviated description of the experimental procedure is provided here.

Intra-ocular recordings were made from anesthetized and paralyzed cats in response to spots of various sizes, presented at high contrast against a background illumination of ~0.4 cd-m^{-2}. Each spot of a given size was presented 20 times for a period of three seconds. For each spot size, the total spike record across all trials was divided into 200 equally spaced, non-overlapping segments, from 50-300 msec in length. For purposes of this study, these 200 spike train segments were treated as independent stimulus trials.

Model I: Rate-Modulated Poisson Process:

Artificial spike trains were generated under the assumption that the spatiotemporal correlations between cat ganglion cells are due to a common oscillatory input that uniformly modulates the firing rates of all simultaneously recorded neurons. An oscillatory time series of a duration, T, and temporal resolution, Δt, could be constructed by first defining the discrete frequencies, f_k:

$$f_k = \frac{k}{T}, 0 \le k < \frac{T}{\Delta t} \quad (1)$$

in terms of which the discrete Fourier coefficients were defined as follows:

$$C_k = e^{2\pi i r} \exp\left(\frac{(f_k - f_0)^2}{2\sigma^2} \right) \tag{2}$$

where f_0 is the central oscillation frequency, σ is the width of the spectral peak in the associated power spectrum and r is a uniform random deviate between 0 and 1 that randomized the phases of the individual Fourier components (generated by the Matlab® intrinsic function RAND). These coefficients were used to convert back to the time domain using the discrete inverse Fourier transform:

$$R_n = A \frac{1}{N} \sum_{k=1}^{N-1} C_k e^{-2\pi i f_k t_n} + R_0 \tag{3}$$

where the real part of R_n denotes the value of the time-dependent firing rate at the discrete times, $t_n = n \cdot \Delta t$, $N = T \cdot \Delta t$, A is an empirically determined scale factor and we have added a constant offset, R_0, which sets the mean firing rate. Values of A reported in the text, given in units of Hz, are expressed relative to the quantity D, the standard deviation of R_n over all n with $A = 1$. Negative values of R_n were truncated at zero and the resulting time series rescaled so that its average value remained equal to R_0. The time series defined by R_n was used to generate oscillatory spike trains via a pseudo-random process:

$$S_n = \theta(R_n \Delta t - r) \tag{4}$$

where $R_n \cdot \Delta t$ is the probability of a spike in the nth time bin, θ is a step function, $\theta(x<0) = 0$, $\theta(x>0) = 1$, and r is again a uniform random deviate. In the limit that $R_n \cdot \Delta t << 1$, the above procedure reduces to a rate-modulated Poisson process. The same time series, R_n, was used to modulate the firing rate of each element contributing to the

artificially-generated multi-unit spike train, thus producing temporal correlations due to shared input.

Model II: Integrate-and-Fire Feedback Circuit:

A second and very different method for generating artificial spike trains used a semi-realistic model of the inner retina. Input to the model was conveyed by an array of external currents proportional to the pixel-by-pixel grayscale value of a two-dimensional image. These external currents directly stimulated the bipolar cells and approximated the light-modulated synaptic input from cone photoreceptors. The bipolar cells produced excitatory postsynaptic potentials in both ganglion cells and amacrine cells according to a random process (Freed, 2000). The axon-bearing amacrine cells were electrically coupled to neighboring ganglion cells and to each other, and made strong inhibitory connections onto the surrounding ganglion cells and axon-bearing amacrine cells (fig. 1). This feedback circuit produced robust oscillations in response to large stimuli. When several ganglion cells were activated by a stimulus, they in turn activated neighboring axon-bearing amacrine cells via gap junctions (Dacey & Brace, 1992; Vaney, 1994; Jacoby et al., 1996). The stimulated cells were then hyperpolarized by the ensuing wave of axon-mediated inhibition, thus setting up the next cycle of the oscillation. Spike generation was modeled as a leaky integrate-and-fire process with a membrane time constant of 5 msec, consistent with published physiological data from cat alpha ganglion cells (O'Brien et al., 2002). The model also contained local non-spiking amacrine cells that generated randomly distributed inhibitory postsynaptic potentials that helped make spontaneous firing asynchronous, but were not otherwise critical for generating

oscillatory spike trains. Further details of model are presented in the appendix. A thorough analysis of the behavior of the model, its robustness with respect to both numerical and physiological parameters and its connection to experimental data, is presented elsewhere (Kenyon et al., 2003).

Figure 1 about here

Correlation Analysis

Using multi-unit spike trains recorded from the cat retina, multi-unit auto-correlograms were computed for each segment, 200 msec in duration, and the individual correlation functions normalized as a fraction of the expected synchrony due to chance, defined as the mean correlation amplitude for delays between 75-100 msec. A correlation amplitude of one thus corresponded to a doubling in the number of correlated events over the expected rate during that trial. By measuring correlations relative to the baseline present during the same trial, it was possible to compensate, in part, for changes in firing activity during the 3 second stimulus presentation. All correlations were lag corrected for edge effects arising from the finite length of the spike train. The single-trial auto-correlograms were averaged to produce a final correlation measure.

A similar analysis was used to measure correlations in artificially generated spike train segments, also 200 msec in duration. However, for the artificially generated segments, correlations were computed separately between all distinct cell pairs contributing to the multi-unit record, and the individual cross-correlations were averaged to produce a multi-unit cross-correlogram that, unlike the individual auto-correlograms, remained finite at zero delay. The multi-unit cross-correlograms measured on each stimulus trial were normalized relative to the expected correlations due to chance and averaged across all stimulus trials. All multi-trial correlation measures used a bin width

of 1 msec. Shift-predictors were not subtracted, as our hypothesis does not depend on whether or not oscillations are phase-locked to the stimulus onset.

Size Discrimination

We assessed the ability to discriminate between small and large stimuli based on the average spectral amplitude in the upper gamma frequency band (75-95 Hz) as extracted from short segments of multi-unit spike train data on single trials. For multi-unit spike trains recorded from the cat retina, individual segments were 50-300 msec in duration and contained approximately 4-5 neurons, the exact number being unknown. Artificially generated spike train segments were 50-400 msec in duration and contained from 1-16 neurons, as indicated. For spike trains generated by the integrate-and-fire retinal model, segments were always extracted from separate stimulus presentations during the plateau portion of the response, beginning 200 msec after stimulus onset. To estimate the average spectral amplitude in the upper gamma band, the multi-unit spike train was Fourier transformed and the mean amplitude of the discrete Fourier coefficients between 75 and 95 Hz was computed. The mean spectral amplitude in the upper gamma band was expressed as a fraction of the mean baseline spectral amplitude, defined here as the average between 120 and 500 Hz, computed on the same trial. This normalization had little consequence for artificially generated spike trains, but was necessary to compensate for the changing baseline of the experimentally recorded data. The average spectral amplitude in the upper gamma band was determined for each segment and the results expressed as a probability distribution. The percentage of trials on which an the stimulus could be correctly classified as being either "small" or "large" was inversely related to the degree of overlap between the probability distributions for the two stimulus sizes. Total overlap corresponded to performance at chance (50% correct) while zero overlap indicated perfect discrimination (100% correct).

Results

As reported previously (Neuenschwander et al., 1999), multi-unit auto-correlograms recorded from cat retinal ganglion cells exhibited high frequency oscillations whose amplitude increased markedly with stimulus size (fig. 2a). A small square spot, 0.7°×0.7°, produced negligible oscillations, while a large square spot, 9.8°×9.8°, evoked strong oscillations at approximately 80 Hz. An intermediate sized spot, 6.3°×6.3°, produced periodic correlations at similar frequencies to those elicited by the larger spot but of smaller amplitude and duration, indicating that over this range of spot dimensions oscillatory responses depend smoothly on stimulus size. Periodic modulations in the multi-unit auto-correlogram declined with increasing delay, indicating that the oscillation phase drifted randomly over time. The multi-unit auto-correlogram is undefined at zero delay and was set arbitrarily to zero.

Figure 2 about here

Multi-unit cross-correlograms computed from spike trains produced by either by a simple rate-modulated Poisson process (model I, fig. 2b) or with a semi-realistic retinal feedback circuit (model II, fig. 2c) exhibited oscillations whose size dependence, amplitude, duration and frequency were similar to those measured experimentally. For the rate-modulated Poisson process, the amplitude and width of the spectral peak were adjusted to produce a good qualitative fit with the physiological data for each spot size (A = 0, 31.5, 50 Hz, σ = 15, 9.5, 6.25 Hz, for the small, intermediate, and large spots, respectively. The mean firing rate, R_0, was 50 Hz.). For the integrate-and-fire feedback circuit, we used square spots covering either 1×1, 4×4, or 6×6 ganglion cells (stimulus

intensity = 0.25). Poisson distributed events were added to the spike trains generated by the retinal model, as necessary, to ensure that the mean firing rate was always 50 Hz regardless of stimulus size. Both of the artificially generated event trains consisted of 4 units, which in the case of the retinal model were taken from a 2×2 array of neighboring ganglion cells located at the center of the stimulus.

To quantify the dependence of oscillatory responses on stimulus size, we Fourier analyzed 200 msec epochs of both natural and artificial multi-unit spike trains, using the same data as for the above correlation analysis. The magnitudes of the Fourier coefficients computed from individual spike train segments were normalized by the total number of events, given by the Fourier coefficient at 0 Hz, and the results from all 200 stimulus trials averaged together (fig. 3). In all three sets of data, a prominent peak in the upper gamma frequency band, approximately 75-95 Hz, became evident as the size of the stimulus increased. Previous studies have shown that high frequency oscillations between spatially disconnected stimuli are not coherent (Neuenschwander & Singer, 1996), implying that if the large spot were broken up into multiple small fragments, the prominent peak in the upper gamma frequency band would be abolished.

Figure 3 about here

Measures of oscillatory responses among retinal ganglion cells presented so far, either multi-unit correlograms or frequency spectra, are all based on averages over multiple trials. Such multi-trial measures are not available to the animal's nervous system, however. For retinal oscillations to be behaviorally relevant, they must be detectable on physiological time scales, roughly 10s to 100s of msec. Furthermore, the relatively low convergence from the retina onto targets early in the visual processing

pathway imposes constraints on the size of the ganglion cell population that should be included in the analysis. Consistent with these constraints, there were approximately 4-5 ganglion cells in the multi-unit spike trains recorded from the cat retina and the artificially generated spike trains contained exactly 4 units. To examine the detectability of retinal oscillations, we computed averages of normalized frequency spectra in the upper gamma band, 75-95 Hz, relative to the averaged spectral amplitude between 120-500 Hz present during the same 200 msec epoch. The analysis was repeated for all 200 epochs and the results presented as a probability distribution for each stimulus size (fig. 4). For both natural and artificial spike trains, there is relatively little overlap between the distributions for the smallest and largest stimuli, implying that gamma-band oscillations from a small group of neighboring ganglion cells permit good single-trial discrimination.

Figure 4 about here

To quantify the degree of discrimination theoretically possible on single stimulus trials, we employed a Bayes discriminator (Duda et al., 2001). Using the probability distributions shown above, we found that 200 msec segments of multi-unit spike trains from the cat retina permit discrimination between larger and small spots on more than 80% of the trials (fig. 5a). Thus, the average spectral amplitude in the upper gamma band across a small number of neighboring ganglion cells conveyed enough information on behaviorally relevant time scales to determine whether the recorded neurons were responding to a small or large stimulus. The artificially generated spike trains yielded slightly better performance on the size discrimination task, exceeding 90% correct for both models (fig. 5b,c). The artificially generated spike trains all had the same mean

firing rate regardless of stimulus size, showing that differences in the total number of spikes were irrelevant to the size discrimination task.

It is uncertain why the spike trains generated artificially yielded better performance then those recorded experimentally. One explanation is that the experimentally recorded spike trains may have included ganglion cells of different types and opposite ON/OFF response polarities whereas the computer generated spike trains were derived from a homogeneous population. The changing baseline of the experimentally recorded spikes trains may also have confounded the discrimination analysis, despite efforts to correct for non-stationary effects. Thus, the performance levels obtained with the experimentally recorded data likely reflect a lower bound on the maximum performance levels theoretically attainable.

Figure 5 about here

We next examined how the information about the stimulus size encoded by retinal oscillations depends both on the length of, and number of neurons contributing to, the multi-unit spike record. Performance on the size discrimination task, as measured by the percentage of correctly classified trials in which either the small or the large spot was presented with equal probability, was plotted as a function of the analysis window size. For the artificially generated spike trains, the analysis used either 1×1, 2×2, 3×3, or 4×4 neurons, corresponding to 1, 4, 9, or 16 total cells, respectively (fig. 6). For simultaneously recorded cat ganglion cells, performance ranged from approximately 70-90% as the analysis window size increased from 50 to 300 msec. Both theoretical models suggested that the information content of simultaneously recorded spike trains depends strongly on the number of cells included in the multi-unit record. Even for

analysis windows as short as 50 msec, performance levels of 80% or better could be achieved by including a sufficient number of cells. The ability to extract topological information from 50 msec spike train segments was particularly evident for the rate-modulated Poisson process, while artificial spike trains generated by the retinal model conveyed substantially less size information on short time scales. This discrepancy may be related to the synchronization of neighboring ganglion cells in the retinal model due to their extensive gap junction coupling via amacrine cells. In both models, performance levels at or above 80% could be achieved with only four units in approximately 100 msec, a result consistent with the low convergence at early visual processing stages.

Figure 6 about here

Discussion

We have examined the role of ganglion cell oscillations in the encoding of visual information. Our analysis shows that high frequency oscillations in small groups of neighboring ganglion cells allow single-trial discrimination between large and small spots on biologically reasonable time scales. This single trial discrimination is essential if synchronous oscillations between retinal neurons are to convey behaviorally relevant stimulus attributes to early visual processing stages. Similar single trial discrimination was observed in two very different theoretical models whose multi-trial correlations were both consistent with experimental data, suggesting that the information conveyed by coherent oscillations is not strongly dependent on the underlying physiological mechanisms giving rise to the oscillations. In particular, similar single trial discrimination was obtained regardless of whether temporal correlations were produced by periodically modulated common input or through the dynamics of synaptically mediated feedback loops.

Ganglion cell firing rates are strongly modulated by local stimulus properties, such as contrast. The average firing rate among a small group of neighboring ganglion cells cannot therefore convey information about global stimulus properties without being confounded by local attributes. High frequency oscillations, on the other hand, are not evoked by small spots, even at high contrast. Thus, oscillations among a small group of neighboring ganglion cells can reliably signal that the stimulus to which they are responding is part of a large feature extending beyond their central receptive fields. High frequency oscillations therefore allow global topological information to be encoded by local spiking activity.

Encoding the presence of a large visual feature early in the visual system has potential behavioral advantages. For many organisms large objects represent possible danger and early detection allows for an early evasive response. It is possible, for instance, that high frequency oscillations between dimming detectors in the frog retina contribute to just such an early warning system (Ishikane et al., 1999). Likewise, in weakly electric fish, synchronized oscillations allow discrimination between prey and communication signals (Doiron et al., 2003). The question of how oscillatory information might be decoded by downstream networks is beyond the scope of the present study. However, we may imagine that corresponding high frequency resonances, of cellular, synaptic and/or network origin might cause neural circuits in the LGN or primary visual cortex to respond preferentially to oscillatory input.

The role of correlations in the neural code is controversial. Using an information theoretic analysis it has recently been argued that correlations between retinal ganglion cells encode relatively small amounts of additional information about natural visual scenes compared to their independent firing rates (Nirenberg et al., 2001). These results are not inconsistent with our work as their analysis used a 10ms time window in which it is impossible to resolve oscillations in the upper gamma band. In addition, the role of synchrony as a possible binding mechanism has sparked intense debate (Singer & Gray, 1995; Shadlen & Movshon, 1999). Our results suggest that oscillations may encode global stimulus information regardless of their possible contribution to feature binding. Finally, it has been observed that any correlation between neural spike-trains is detrimental to rate-coded signals (Shadlen & Newsome, 1998). Correlations, however, are ubiquitous throughout the brain and our results demonstrate that, at least in some

cases, temporal correlations convey potentially useful information not present in the local firing rates.

Appendix

Retinal Model

Artificial spike trains with realistic spatiotemporal correlations were generated by a retinal feedback circuit (fig 1), organized as a 32×32 array with wrap-around boundary conditions containing 5 distinct cell types: Bipolar cells, small amacrine cells, large amacrine cells, axon-bearing amacrine cells, and ganglion cells. All cell types were modeled as single compartment, RC circuit elements obeying a first order differential equation that can be written efficiently in terms of matrix multiplications:

$$\dot{\vec{V}}^{(k)} = -\frac{1}{\tau^{(k)}}\left(\vec{V}^{(k)} - \sum_{k'} \vec{W}^{(k,k')} \cdot f^{(k,k')}\left(\vec{V}^{(k')}\right) \cdot \vec{W}^{(k,k')^T} - b^{(k)} - \vec{L}^{(k)} \right), \qquad \text{(A1)}$$

where $\vec{V}^{(k)}$ is a 2-D array denoting the normalized membrane potentials of all cells of type k, $(1 \le k \le 5)$, $\tau^{(k)}$ is the time constant, $b^{(k)}$ is a bias current for setting the resting potential, $\vec{L}^{(k)}$ is an external input intended to represent light stimulation, $\vec{W}^{(k,k')}$ gives the connection strengths between presynaptic $\{k'\}$ and postsynaptic $\{k\}$ cell types as a function of their separation along one direction, defined here as 'vertical', $\vec{W}^{(k,k')^T}$ gives the same information as a function of separation along the perpendicular direction, defined here as 'horizontal', and the functions $f^{(k,k')}$ give the associated input-output relations for the indicated pre- and post-synaptic cell types, detailed below. All membrane potentials were subject to a lower cutoff, equal to –1.5. The output of the axon-mediated inhibition was delayed by 2 msec, except for the axonal connections onto the axon-bearing amacrine cells, which was delayed for 1 msec. All other synaptic interactions were delayed by 1 msec. All equations were integrated in Matlab® using a direct Euler method with an integration time step of 1 msec.

The input-output function for gap junctions was given by the identity:

$$f^{(k,k')}\left(\vec{V}^{(k')}\right) = \vec{V}^{(k')}, \qquad \text{(A2)}$$

where the dependence on the presynaptic potential has been absorbed into the definition of $\tau^{(k)}$. This is possible because both the decay term in equation A1 and the omitted dependence on the presynaptic potential in equation A2 depend linearly on $\vec{V}^{(k)}$, allowing the coefficients to be combined. The input-output function for non-spiking synapses was constructed by comparing, on each time step, a random number with a Fermi-function:

$$f^{(k,k')}\left(\vec{V}^{(k')}\right) = \theta\left(\left[\frac{1}{1+\exp\left(-\alpha\vec{V}^{(k')}\right)}\right] - r\right), \tag{A3}$$

where α sets the gain (equal to 4 for all non-spiking synapses), *r* is a uniform random deviate equally likely to take any real value between 0 and 1, and θ is a step function, $\theta(x) = 1,\ x \geq 0\ ;\ \theta(x) = 0,\ x < 0$.

Lastly, the input-output relation used for spiking synapses was:

$$f^{(k,k')}\left(\vec{V}^{(k')}\right) = \theta\left(\vec{V}^{(k')}\right). \tag{A4}$$

A modified integrate-and-fire mechanism was used to model spike generation. A positive pulse (amplitude = 10.0) was delivered to the cell on the time step after the membrane potential crossed threshold, followed by a negative pulse (amplitude = -10.0) on the subsequent time step. This resulted in a 1 msec action potential that also produced impulse responses in electrically coupled cells, an important element of the circuit dynamics. The bias current, *b*, was incremented by -0.5 following each spike, and then decayed back to the resting value with the time constant of the cell, adding to the relative refractory period. There was in addition an absolute refractory period of 1 msec.

Along both the horizontal and vertical directions, synaptic strengths fell off as Gaussian functions of the distance between the pre- and post-synaptic cells. For a given horizontal separation, the horizontal weight factor was determined by a Gaussian function of the following form:

$$W_{i^{(k)},j^{(k')}}^{(k,k')} = \alpha\sqrt{W^{(k,k')}}\exp\left[-\frac{\left\|i^{(k)} - j^{(k')}\right\|^2}{2\sigma^2}\right] \quad \text{(A5)}$$

where $W_{i^{(k)},j^{(k')}}^{(k,k')}$ is the horizontal weight factor from presynaptic cells of type k' located in the j^{th} column to the postsynaptic cells of type k located in the i^{th} column, α is a normalization factor, determined numerically, which ensured that the total synaptic input integrated over all presynaptic cells of type k' to every postsynaptic cell of type k equaled $W^{(k,k')}$, σ is the Gaussian radius of the interaction, and the quantity $\left\|i^{(k)} - j^{(k')}\right\|$ denotes the horizontal distance between the pre- and post-synaptic cells, taking into account the wrap around boundary conditions employed to mitigate edge effects. An analogous weight factor describes the dependence on vertical separation. Equation A5 was augmented by a cutoff condition that prevented synaptic interactions beyond a specified distance, determined by the radius of influence of the presynaptic outputs and the postsynaptic inputs, roughly corresponding to the axonal and dendritic fields, respectively. A synaptic connection was only possible if the output radius of the presynaptic cell overlapped the input radius of the postsynaptic cell. Except for axonal connections, the input and output radii were the same for all cell types. For the large amacrine cells and the ganglion cells, the radius of influence extended out to the centers of the nearest neighboring cells of the same type, producing a coverage factor greater than one (Vaney, 1990). The radii of the bipolar, small, and axon-bearing amacrine cells (non-axonal connections only) extended only halfway to the nearest cell of the same type, giving a coverage factor of one (Cohen & Sterling, 1990). The external input was multiplied by a gain factor of 3. Values for model parameters are listed in tables 1 and 2. A more complete description of the model is presented elsewhere (Kenyon et al., 2003).

Table 1: Cellular parameters.

	τ	b	n×n	d	σ
BP	10.0	-0.0	64×64	0.25	0.25
SA	25.0	-0.5	64×64	0.25	0.25
LA	20.0	-0.25	32×32	1.0	0.5
PA	5.0	-0.025	64×64	0.25/9.0[a]	0.25/3.0[a]
GC	5.0	-0.025	32×32	1.0	0.5

Explanation of symbols: τ: time constant (msec); b: bias; n×n: array size; d: cutoff radius, σ: Gaussian radius (see eq. 5). [a]Inner radius/outer radius.

Table 2: Synaptic weights.

	BP	SA	LA	PA	GC
BP	*	-0.375[b]-	3.0b	-3.0b/-15.0c	*
SA	3.0[b]	*	-3.0[b]	0.0b/-15.0[c]	*
LA	3.0[b]	*	0.25[a]	-3.0a/-15.0[c]	*
PA	0.75[b]	-0.75b	0.25[a]	0.25a/-45.0[c]	0.25[a,d]
GC	9.0[b]	-4.5b	-4.5[b]	0.25[a]/-270.0[c]	*

Each term represents the total integrated weight from all synapses arising from the corresponding presynaptic type (columns) to each cell of the corresponding postsynaptic type (rows), (the quantity $W^{(k,k')}$ in eq. 5). Asterisk (*) indicates absence of corresponding connection. Synapse type indicated by superscript: [a]gap junction, [b]non-spiking synapse, [c]spiking synapse. [d]Maximum coupling efficiency (ratio of post- to pre-synaptic depolarization) for this gap junction synapse: DC=11.3%, Action Potential=2.7%.

Figure Captions

Figure 1. Schematic of the retinal feedback circuit. Only those elements directly responsible for synchronous oscillations are depicted. A combination of local excitation via gap junctions (resistors) and long-range inhibition via axon-bearing amacrine cells (gray dotted lines and filled black circles) produced physiologically realistic size-dependent oscillations. The entire model contained a 32×32 array of ganglion cells driven by a 64×64 array of bipolar cells, with inhibitory feedback arising from a 64×64 array of axon-bearing amacrine cells, only a few of which are shown. Light stimuli were implemented by injecting currents directly into bipolar cells.

Figure 2. Multi-unit auto- and cross-correlograms reveal size-dependent high frequency oscillations. a) Auto-correlograms computed from multi-unit spike trains recorded from cat retina at the center of square spots of increasing size (data replotted from (Neuenschwander et al., 1999)). Correlations expressed as a fraction of the expected level due to chance. Bottom Trace: spot size = 0.7º×0.7º. Middle Trace: spot size = 6.3º×6.3º. Top Trace: spot size = 9.8º×9.8º. Individual traces are offset by 2 units for clarity. (b) Multi-unit cross-correlograms of artificial spike trains generated by a Poisson process containing 4 identically modulated units, each with a mean firing rate of 50 Hz. c) Multi-unit cross-correlograms produced by an integrate-and-fire feedback circuit consistent with retinal anatomy. The retinal model was stimulated by stationary spots (intensity = -2) covering 1×1, 4×4 and 6×6 ganglion cells. Multi-unit spike-trains were recorded from a fixed 2×2 array of ganglion cells located at the center of each spot.

Poisson distributed spikes were added to each train to maintain a constant mean firing rate of 50 Hz regardless of spot size.

Figure 3. Frequency spectra of natural and artificial multi-unit spike trains as a function of spot size. Same data and general organization as in figure 2. a) Frequency spectra, normalized by the total number of spikes, computed from multi-unit spike trains recorded from the cat retina in response to different sized spots. b) Normalized frequency spectra of multi-unit spike trains generated by a rate-modulated Poisson process. c) Normalized frequency spectra of multi-unit spike trains produced by the retinal feedback circuit. In all panels, a prominent peak in the upper gamma band, roughly 75-95 Hz, becomes evident as spot size increases.

Figure 4. Distribution of the mean spectral amplitude in the upper gamma band across individual 200 msec segments of multi-unit firing activity. Same data as in figures 2 and 3. Average Fourier amplitude in the upper gamma band, between 75 and 95 Hz, was measured relative to the average baseline amplitude between 120 and 500 Hz. Results distributed among 11 uniform bins (arbitrary units). a) Distribution of average gamma spectral amplitude in short multi-unit spike trains recorded from cat retinal ganglion cells. The distribution of gamma amplitudes elicited by a small spot (dotted line) is largely distinguishable from that elicited by both intermediate (dashed line) and large spots (solid line). b) Distribution of gamma amplitudes in multi-unit spike trains produced by a rate-modulated Poisson process. c) Analogous distribution arising from retinal feedback circuit. In both sets of artificially generated spike trains, the distributions of gamma

amplitudes associated with different spot sizes are clearly distinct, suggesting that the information content of the oscillations does not depend strongly on the underlying mechanism giving rise to them.

Figure 5. Theoretically optimal performance on a size discrimination task. Individual 200 msec segments of multi-unit spike train data were obtained in response to spots of one of two sizes: 1) either an intermediate or small spot (top abscissa = 6.3º×6.3º, bottom abscissa = 4×4) or 2) either a large or small spot (top abscissa = 9.8º×9.8º, bottom abscissa = 6×6). The ordinate gives the maximum percentage of trials that could be classified correctly, assuming each binary possibility was equally likely *a priori*, based on the distributions shown in figure 4. All three data sets indicate that high frequency oscillations within a small group of ganglion cells yield good single trial discrimination of stimulus size.

Figure 6. Size-discrimination improves as multi-unit spike train segments become longer and/or include more cells. An ideal observer was used to discriminate between multi-unit spike records produced by either a small or a large spot. a) Maximum percentage of correctly classified trials plotted as a function of the analysis window size for multi-unit spike trains recorded from cat retinal ganglion cells. Performance levels ranged from approximately 70 to 90% as the length of the multi-unit spike train segment increased from 50 to 300 msec. b) Percent of correctly classified trials using multi-unit spike trains generated by a rate-modulated Poisson process. Performance improved with longer analysis windows and as more units were included in the spike record. (Explanation of

symbols: ○=1, □=4, ◊=9, ×=16 units). c) Percentage of correctly classified trials using multi-unit spike trains generated by the retinal feedback circuit. (Explanation of symbols: ○=1×1, □=2×2, ◊=3×3, ×=4×4 model ganglion cells). Performance was again strongly dependent on the analysis window size and on the number of neighboring ganglion cells included in the analysis.

References

Ariel, M., Daw, N.W. & Rader, R.K. (1983). Rhythmicity in rabbit retinal ganglion cell responses. Vision Research 23(12): 1485-93.

Cohen, E. & Sterling, P. (1990). Convergence and divergence of cones onto bipolar cells in the central area of cat retina. Philosophical Transactions of the Royal Society of London - Series B: Biological Sciences 330(1258): 323-8.

Dacey, D.M. & Brace, S. (1992). A coupled network for parasol but not midget ganglion cells in the primate retina. Visual Neuroscience 9(3-4): 279-90.

De Carli, F., Narici, L., Canovaro, P., Carozzo, S., Agazzi, E. & Sannita, W.G. (2001). Stimulus- and frequency-specific oscillatory mass responses to visual stimulation in man. Clin Electroencephalogr 32(3): 145-51.

Doiron, B., Chacron, M.J., Maler, L., Longtin, A. & Bastian, J. (2003). Inhibitory feedback required for network oscillatory responses to communication but not prey stimuli. Nature 421(6922): 539-43.

Duda, R.O., Hart, P.E. & Stork, D.G. (2001). Pattern Classification. NY, Wiley.

Freed, M.A. (2000). Rate of quantal excitation to a retinal ganglion cell evoked by sensory input. J Neurophysiol 83(5): 2956-66.

Frishman, L.J., Saszik, S., Harwerth, R.S., Viswanathan, S., Li, Y., Smith, E.L., 3rd, Robson, J.G. & Barnes, G. (2000). Effects of experimental glaucoma in macaques on the multifocal ERG. Multifocal ERG in laser-induced glaucoma. Doc Ophthalmol 100(2-3): 231-51.

Ishikane, H., Kawana, A. & Tachibana, M. (1999). Short- and long-range synchronous activities in dimming detectors of the frog retina. Vis Neurosci 16(6): 1001-14.

Jacoby, R., Stafford, D., Kouyama, N. & Marshak, D. (1996). Synaptic inputs to ON parasol ganglion cells in the primate retina. Journal of Neuroscience 16(24): 8041-56.

Kenyon, G.T., Moore, B., Jeffs, J., Denning, K.S., Stephens, G.S., Travis, B.J., George, J.S., Theiler, J. & Marshak, D.W. (2003). A model of high frequency oscillatory potentials in retinal ganglion cells. Visual Neuroscience (in press).

Laufer, M. & Verzeano, M. (1967). Periodic activity in the visual system of the cat. Vision Res 7(3): 215-29.

Neuenschwander, S., Castelo-Branco, M. & Singer, W. (1999). Synchronous oscillations in the cat retina. Vision Res 39(15): 2485-97.

Neuenschwander, S. & Singer, W. (1996). Long-range synchronization of oscillatory light responses in the cat retina and lateral geniculate nucleus. Nature 379(6567): 728-32.

Nirenberg, S., Carcieri, S.M., Jacobs, A.L. & Latham, P.E. (2001). Retinal ganglion cells act largely as independent encoders. Nature 411(6838): 698-701.

O'Brien, B.J., Isayama, T., Richardson, R. & Berson, D.M. (2002). Intrinsic physiological properties of cat retinal ganglion cells. J Physiol 538(Pt 3): 787-802.

Shadlen, M.N. & Movshon, J.A. (1999). Synchrony unbound: a critical evaluation of the temporal binding hypothesis. Neuron 24(1): 67-77, 111-25.

Shadlen, M.N. & Newsome, W.T. (1998). The variable discharge of cortical neurons: implications for connectivity, computation, and information coding. J Neurosci 18(10): 3870-96.

Singer, W. & Gray, C.M. (1995). Visual feature integration and the temporal correlation hypothesis. Annual Review of Neuroscience 18: 555-86.

Steinberg, R.H. (1966). Oscillatory activity in the optic tract of cat and light adaptation. J Neurophysiol 29(2): 139-56.

Vaney, D.I. (1990). The mosaic of amacrine cells in the mammalian retina. Progress in Retinal Research. Osborne, N.N. & Chader, G.J. Oxford, Pergamon Press. 9**:** 49-100.

Vaney, D.I. (1994). Patterns of neuronal coupling in the retina. Progress in Retinal and Eye Research 13: 301-355.

Wachtmeister, L. (1998). Oscillatory potentials in the retina: what do they reveal. Prog Retin Eye Res 17(4): 485-521.

Wachtmeister, L. & Dowling, J.E. (1978). The oscillatory potentials of the mudpuppy retina. Invest Ophthalmol Vis Sci 17(12): 1176-88.

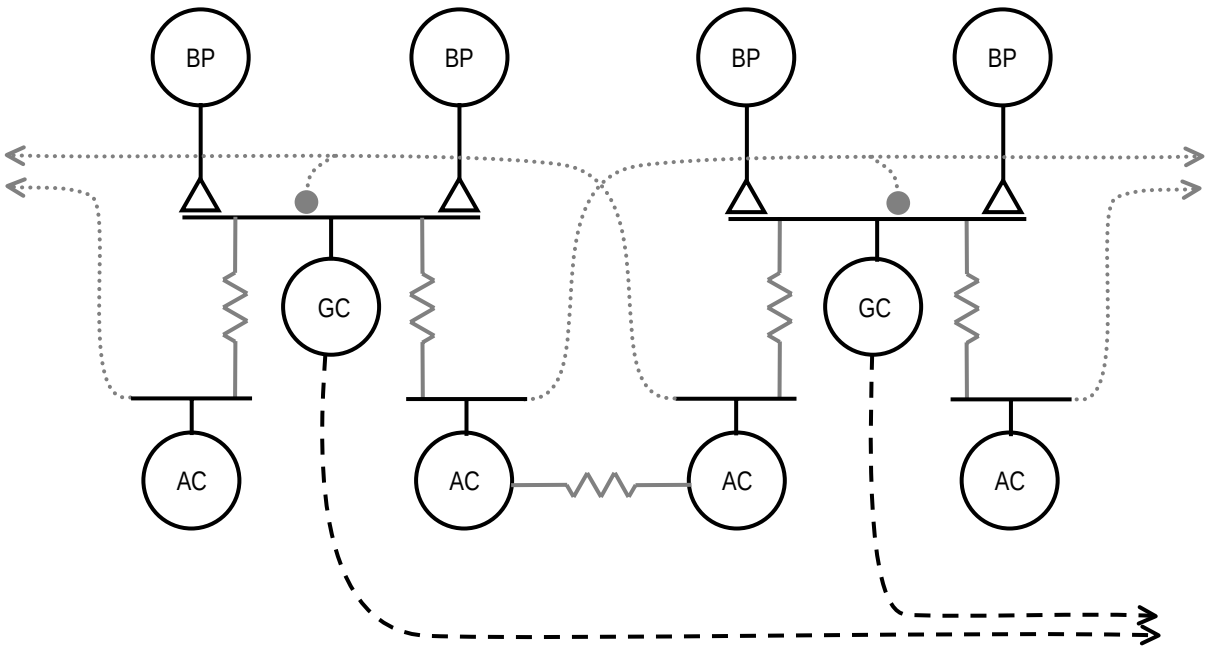

Fig 1

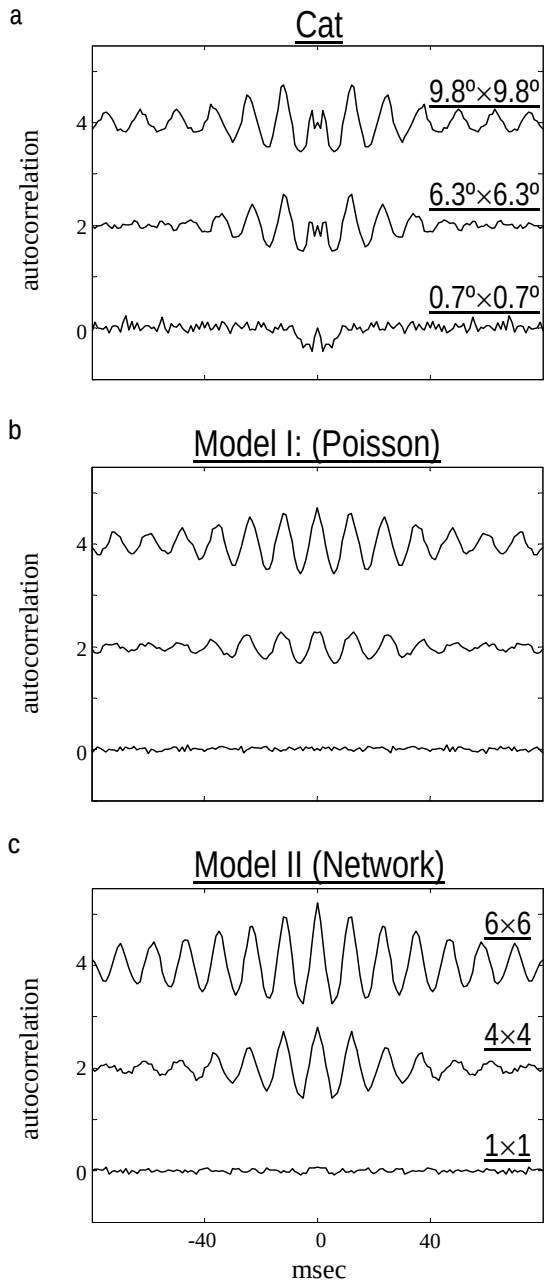
a
Cat
9.8º×9.8º
6.3º×6.3º
0.7º×0.7º
autocorrelation
4
2
0
b
Model I: (Poisson)
autocorrelation
4
2
0
c
Model II (Network)
6×6
4×4
1×1
autocorrelation
4
2
0
-40
0
40
msec

Fig 2

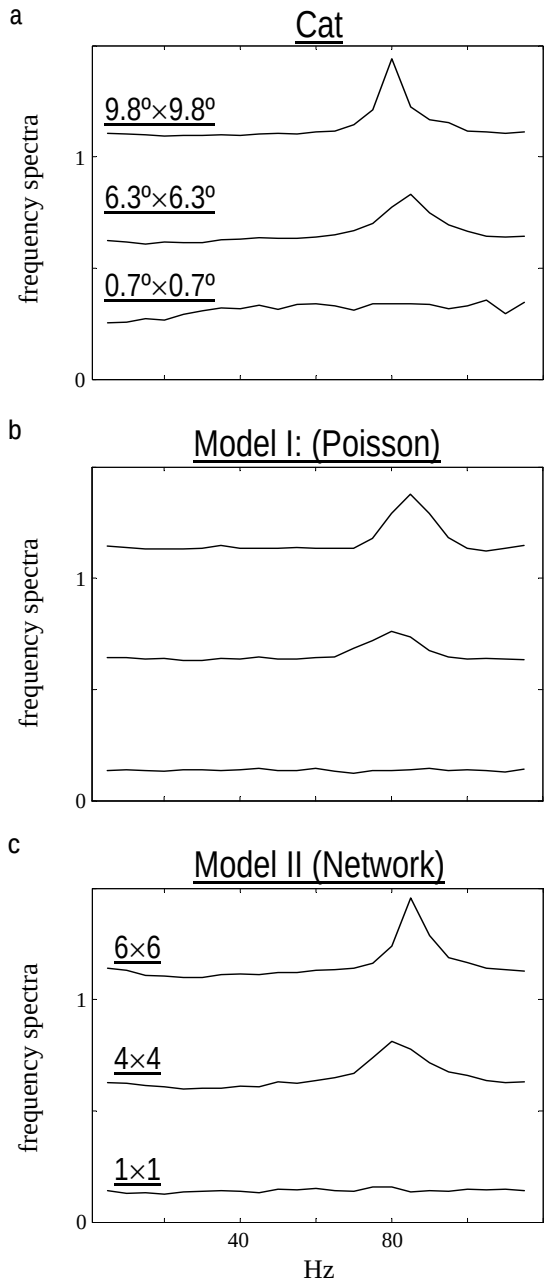
a
Cat
9.8º×9.8º
6.3º×6.3º
0.7º×0.7º
frequency spectra
1
0
b
Model I: (Poisson)
frequency spectra
1
0
c
Model II (Network)
6×6
4×4
1×1
frequency spectra
1
0
40
80
Hz

Fig 3

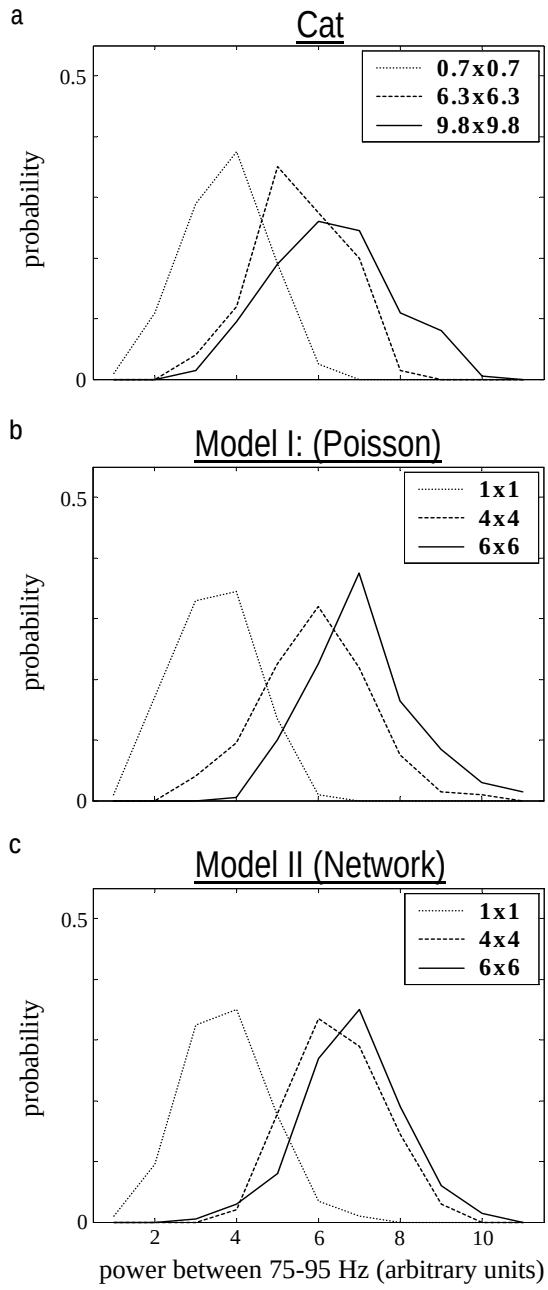
a
Cat
0.7x0.7
6.3x6.3
9.8x9.8
probability
0.5
0
b
Model I: (Poisson)
1x1
4x4
6x6
probability
0.5
0
c
Model II (Network)
1x1
4x4
6x6
probability
0.5
0
2
4
6
8
10
power between 75-95 Hz (arbitrary units)

Fig 4

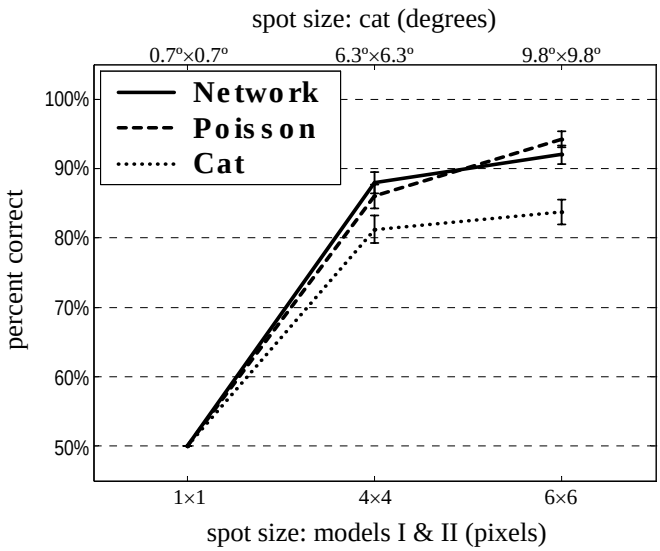
spot size: cat (degrees)
0.7°×0.7°
6.3°×6.3°
9.8°×9.8°
Network
Poisson
Cat
100%
90%
80%
70%
60%
50%
percent correct
1×1
4×4
6×6
spot size: models I & II (pixels)

Fig 5

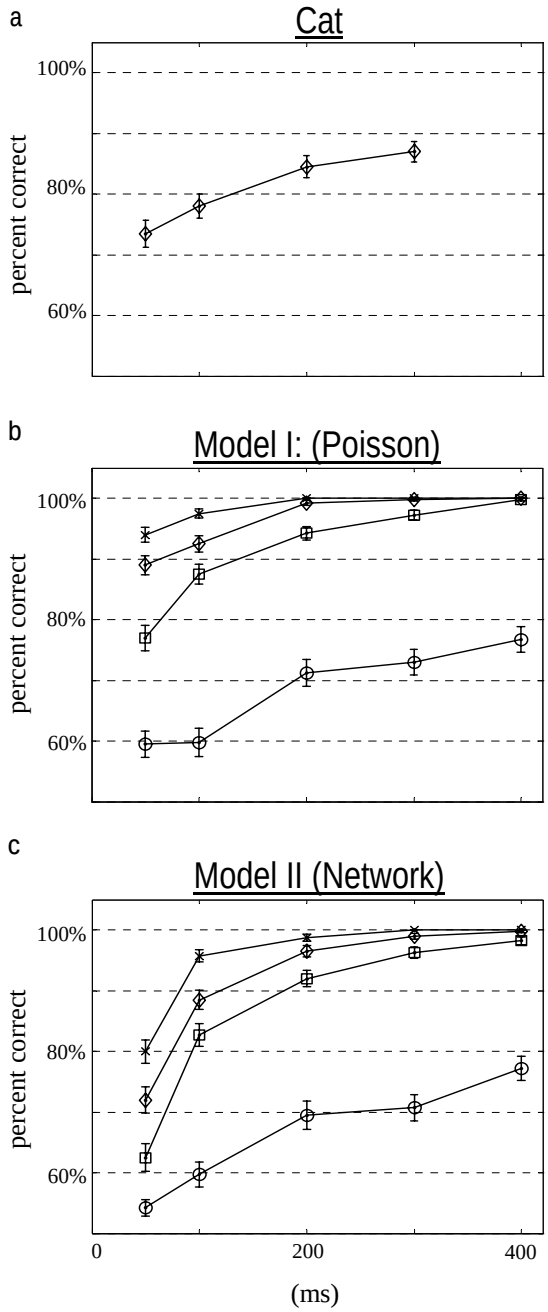
a
Cat
100%
80%
60%
percent correct
b
Model I: (Poisson)
100%
80%
60%
percent correct
c
Model II (Network)
100%
80%
60%
percent correct
0
200
400
(ms)

Fig 6